



## Microstructure evolution of depleted uranium impacted by steel projectile at velocity of 50 m/s

Dong-li ZOU, Ya-kun GUO, Mao-bing SHUAI, Da-wu XIAO

Institute of Materials, China Academy of Engineering Physics, Jianguo 621907, China

Received 22 January 2016; accepted 17 August 2016

**Abstract:** The deformed microstructure evolution of depleted uranium impacted by steel projectile at a velocity of 50 m/s was investigated by means of confocal laser scanning microscope, electron backscatter diffraction, transmission electron microscope and indenter technique. The experimental results showed that the spherical cap crater was formed in depleted uranium target impacted by steel projectile, and the diameter and depth of the impacted crater were 5.45 and 1.01 mm, respectively. From crater rim to deep matrix, four deformed zones were classified, including twin fragmentation zone, high density deformation twin zone, low density deformation twin zone and matrix zone. Twinning was considered as the dominant plastic deformation mechanism of depleted uranium subjected to impact loadings. Besides twinning, the dislocation slipping also played an important role to accommodate the plastic deformation. Finally, the deformed microstructure evolution of depleted uranium under high velocity impact was proposed.

**Key words:** depleted uranium; steel projectile; dynamic deformation; microstructure evolution; twinning

### 1 Introduction

Depleted uranium (DU) has been widely used in armor and armor penetrating fields due to its high density, high hardness and good self-sharpening property [1]. Broad applications in military fields, DU would be suffered from the impact loadings or shock loadings inevitably. Thus, it is necessary to obtain a fundamental understanding about plastic deformation process of DU subjected to impact loadings. However, high loading strength and short time of impact loadings lead to the real-time observation of dynamic deformation process difficultly [2], thus, the post-deformation microstructure characterization has been used to understand the impact evolution indirectly due to the fact that the deformed microstructures are closely related with the deformation process [3].

High stain rate and large stain provided by the impact loadings lead to appearance of various deformed microstructures in materials, such as dislocation microstructures, deformation twins, recrystallized grains, amorphization. Dislocation microstructures including dislocation cell, wall and microbands under impact loadings have been observed in face centered cubic (FCC)

Al [4], Cu [5], Ni [6] and stainless steel [7]. Deformation twins including primary and secondary twins have been observed and confirmed in stainless steel under dynamic deformation [8]. The mixture microstructures composed of microbands and microtwins have been observed far from the crater in Cu [9] and stainless steel targets [7]. Dynamic recrystallized grains near the crater under high speed impact in Cu and Ni targets have been found by MURR et al [9,10]. Shock-induced localized amorphization in boron carbide has been observed by CHEN et al [11].

Though lots of works have been performed on the deformed microstructures in metals under impact loadings, limited results associated with the deformed microstructure in DU targets are available in previous references, especially microstructure evolution of DU subjected to impact loadings unclearly. Thus, it is necessary to investigate the deformed microstructures of DU under impact loadings. In addition, impact loadings can offer the gradient variation of the strain and strain rate from the crater bottom to the deep matrix, thus, the characterization of the deformed microstructure at different depths provides an important clue to elucidate deformed microstructure evolution of materials subjected to high strain rate and large strain loadings. In this work,

the deformed microstructures at different depths in DU target under high velocity impact were characterized, and the corresponding deformed microstructure evolution of DU from the crater rim to the matrix was proposed.

## 2 Experimental

DU with thickness of about 30 mm was selected as the target. The DU target had the coarse grains with diameter ranging from several hundreds micrometers to several millimeters, and a number of impurities were found in DU target. High velocity impact was carried out on a gas gun using cylindrical penetrating steel projectile. The length and diameter of the penetrating projectile were 100 and 10 mm, respectively, and the spherical head with diameter 10 mm was used to penetrate DU targets. In order to decrease the air contamination and protect the experimenters, much lower impact velocity was used due to the fact that lots of aerocolloids would be produced in the process of uranium targets impacted by steel projectile. The impact velocity measured by laser device of 50 m/s was used in this work. After impact, the targets were sectioned along impact direction, mechanically polished and electrochemically etched in a 5% phosphoric acid water solution operated at 5 V and 30 s. The montage macroscopic views and metallographic microstructure of DU impacted by steel projectile were observed by a confocal laser scanning microscope (CLSM, MRC-1000). The specimens were prepared for EBSD observation using the procedure reported in detail in Refs. [12]. The automated EBSD data collection was performed using a TSL camera attached to a dual beam FIB (FEI Helios NanoLab DualBeam system) at a voltage of 25 kV. Thin sheets for transmission electron microscope (TEM) observation were cut parallel to impact direction, followed by mechanical polishing to a thickness about 50  $\mu\text{m}$ . Final thinning to electron transparency was achieved by double jet polishing in a solution of 10 mL nitric acid +45 mL *n*-butanol + 45 mL methanol. The polishing voltage was kept constant at 30 V and the temperature was kept at

−30 °C. The TEM observation was carried out with a F20 microscope operated at 200 kV. Following optical metallographic observation, Vickers microhardness was measured by microhardness tester. The load of 2 kg and a dwell time of 15 s were employed during microhardness measurement.

## 3 Results and discussion

### 3.1 Impact crater

Macroscopic views of a crater in depleted uranium target impacted by steel projectile at a velocity of 50 m/s are shown in Fig. 1. Severe plastic deformation around the crater can be observed in Fig. 1(a), and a few micro-cracks adjacent to the crater can be found. After high velocity impact, spherical cap crater is formed in DU target, as shown in Fig. 1(b). According to the measurement, the diameter ( $D_c$ ) and depth ( $P_c$ ) of the impacted crater are about 5.45 and 1.01 mm, respectively. High density deformation twins near the crater rim can be observed in Fig. 1(b), indicating that the deformation twin is an important plastic deformation mechanism of DU subjected to impact loadings. The formation of deformation twins in uranium under high velocity impact is associated with the crystal structure and stress levels. The crystal structure of alpha-uranium is orthorhombic (*Cmcm* space group), as shown in Fig. 2, and it is made up of corrugated sheets of uranium atoms parallel to the (010) or *ac* planes[13]. The depth or amplitude of corrugation within each sheet is along the [010] direction and the width of corrugation is along the [001] direction, and the separated distance of the corrugated planes is  $b/2$  [14]. The strong anisotropy of uranium has been reported, and the ideal tensile strengths of uranium single crystal along [100], [010] and [001] were 21.3, 14.9 and 12.8 GPa, respectively [13]. Thus, the strong anisotropy assisted with severe plastic deformation leads to the formation of high density deformation twins [15,16], and the twinning, as an important plastic deformation mode, has been extensively observed and reported in DU under plastic deformation [17,18].

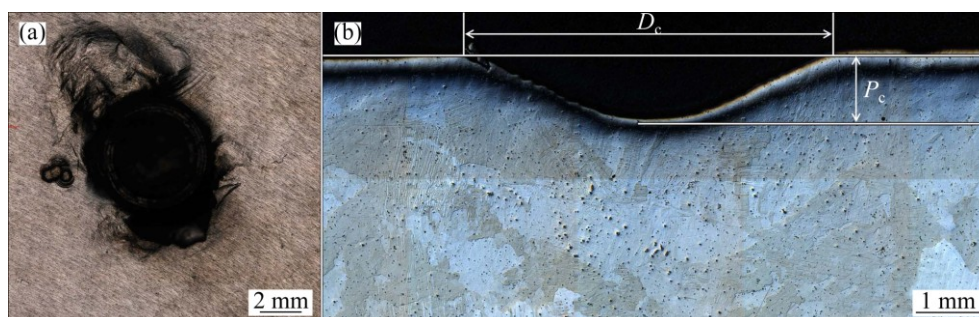


**Fig. 1** Macroscopic views of crater in depleted uranium target impacted by steel projectile at velocity of 50 m/s: (a) Top view; (b) Corresponding cross-section view

### 3.2 Characterization of deformed microstructure

The deformed microstructure distribution under the crater in depleted uranium target impacted by steel projectile at a velocity of 50 m/s is shown in Fig. 3. The montage image of the deformed microstructure from crater rim to deep matrix is shown in Fig. 3(a). It can be seen that the gradient twin variation from the crater rim to deep matrix is confirmed, which should be associated with gradient attenuation of the shock wave during high velocity impact. With increasing the distance from the crater rim, the peak strength and stress level of the shock wave decrease gradually, leading to the formation of the

gradient twin variation from the crater rim to deep matrix. Meanwhile, the grain orientation has an important influence on the twin density. The grains with soft orientation are inclined to form high density deformation twins due to low critical shear stress, while the grains with hard orientation are difficult to form the deformation twins because of high critical shear stress, leading to deformation twin density in grain at the same distance from the crater rim different from each other. According to the deformation twin density, four deformed zones from the crater rim to deep matrix can be classified and divided, including twin fragmentation

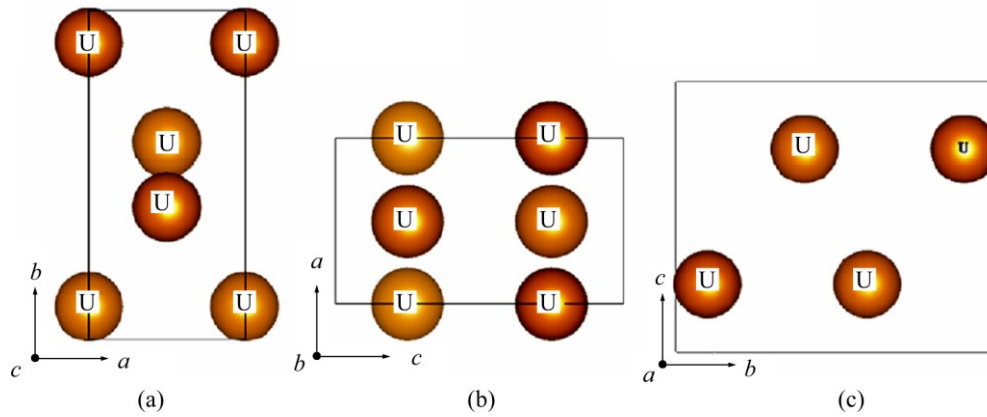


**Fig. 2** Orthorhombic  $C_{2v}$  structure of uranium in unit-cell: (a) Atom projection in  $ab$  plane; (b) Atom projection in  $ac$  plane; (c) Atom projection in  $bc$  plane [13]

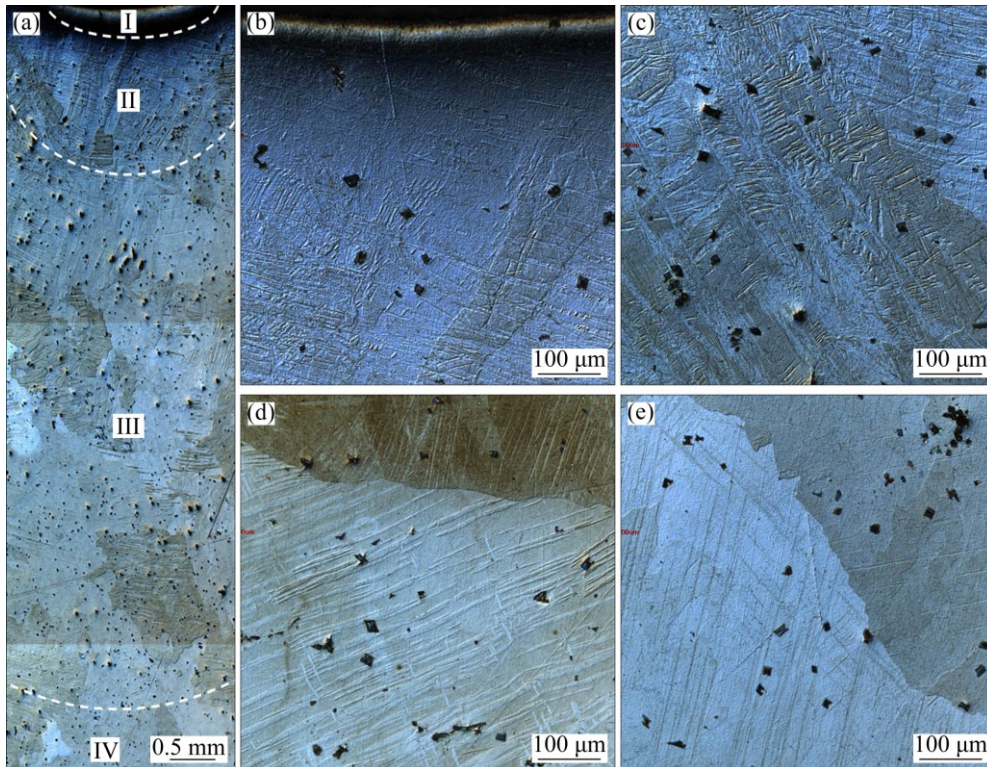


**Fig. 3** Deformed microstructure distribution under crater in depleted uranium target impacted by steel projectile at velocity of 50 m/s: (a) Montage image; (b) Twin fragmentation zone (zone I); (c) High density deformation twin zone (zone II); (d) Low density deformation twin zone (zone III); (e) Matrix zone (zone IV)

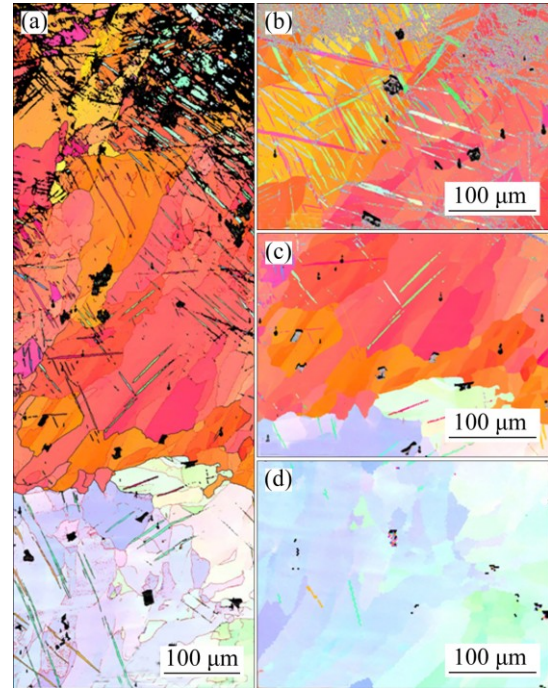
zone (TFZ), high density deformation twin zone (HDDTZ), low density deformation twin zone (LDDTZ) and matrix zone (MZ). OM image of deformed microstructure in TFZ is shown in Fig. 3(b), and the ultrafine and equiaxed grains in local area can be observed in TFZ. Severe plastic deformation assisted with temperature rising leads to the formation of ultrafine grains in localized area in TFZ. In HDDTZ, almost every grain presents high density deformation twins, and high density deformation twins intersect with each other to form the ultrafine twin laths, as shown in Fig. 3(c). The difference between the HDDTZ and LDDTZ is that some grains in LDDTZ present no deformation twins. OM image of deformed microstructure in LDDTZ is shown in Fig. 3(d), and the coarse primary twins crossed through the grains can be observed. In comparison with the HDDTZ, the deformation twin density in LDDTZ decreases dramatically. Far from the crater, only a few coarse primary twin laths can be observed in grains, as shown in Fig. 3(e), indicating that the plastic deformation of the materials in MZ is low.

Figure 4 shows the EBSD images of deformed microstructure under the crater in depleted uranium target. High internal stress caused by severe plastic deformation and fine twin lathes lead to the indexed rate of the TFZ decreasing dramatically. Thus, the EBSD image of deformed microstructure in the TFZ cannot be indexed. The indexed EBSD images of deformed microstructure in the HDDTZ, LDDTZ and MZ are shown in Figs. 4(b)–(d), respectively, and the montage images from HDDTZ to MZ are shown in Fig. 4(a). It can be seen that the gradient twin variation from HDDTZ to MZ can be observed, which is associated with the gradient experimental parameter variation caused by impacting. The gradient stress, strain and temperature fields lead to the formation of the gradient twin distribution. The formation of high density twin laths can be seen in Fig. 4(b), and the intersected twin laths trigger the formation of the two-order, even high-order deformation twins. In LDDTZ and MZ, the twin density decreases obviously, and the primary twins play a dominant role.

### 3.3 Plastic deformation modes

Based on the characterization of deformed microstructures in different zones, the deformation twins are the main plastic deformation mechanism of DU subjected to dynamic loadings. Typical CLSM images of deformation twins in depleted uranium target impacted by steel projectile at a velocity of 50 m/s are shown in Fig. 5. Severe plastic deformation leads to the twin boundaries twisted, which is evidently different from the deformation twins formed at low strain and strain rate

loadings. The twin density and morphology in neighbor grains are different, which should be associated with grain orientation. Besides the coarse primary twins, the intersection of the primary twins leads to the formation of the secondary twins. Compared with the primary twins, the secondary twins become much finer.



**Fig. 4** Deformed microstructure distribution under crater in depleted uranium target impacted at velocity of 50 m/s: (a) Montage image; (b) High density deformation twin zone (zone II); (c) Low density deformation twin zone (zone III); (d) Matrix zone (zone IV)

The EBSD image of deformation twins formed in DU target is shown in Fig. 6(a), and the indexed twin boundary is used to analyze the twin modes. According to the misorientation measurement of the point to point and point to origin, the misorientation between the deformation twin and parent grain is mainly located at 70° and 92°. Typical deformation twins with different misorientations are shown in Figs. 6(d) and (e), and the corresponding grain orientations from parent grain to twin are also shown in Figs. 6(b) and (c). The misorientation between the twin and parent grain in Fig. 6(b) is 72.2° about the  $\langle 10\bar{1}2 \rangle$  axis, and the lattice planes of the parent grain and twin are  $(4\bar{1}6\bar{5})$  and  $(\bar{1}2258)$ , respectively. The measure misorientation from the parent grain to twin along line C in Fig. 6(b) is shown in Fig. 6(d), and the misorientation about 70° between the parent grain and twin is confirmed. As reported, the  $\{130\}$  twin with the misorientation between the twin and parent grain is 69° about the  $\langle 001 \rangle$  axis [19], showing that the deformation twin formed in Fig. 6(b) is the  $\{130\}$  twin, a tolerance of 3.2° from the ideal misorientation

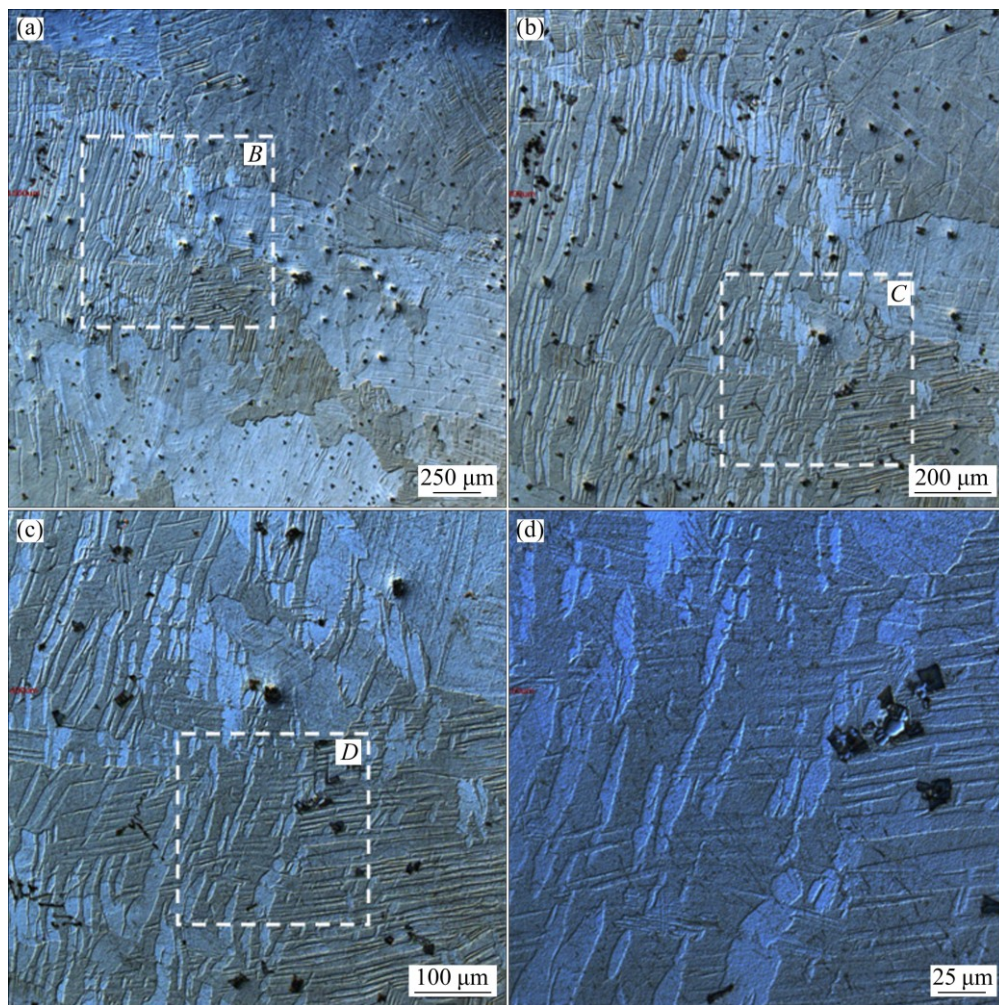


**Fig. 5** CLSM images of deformation twins in depleted uranium target impacted by steel projectile at velocity of 50 m/s: (a) Low magnified image; (b–d) High magnified images in zones *B*, *C* and *D*, respectively

relationship. Furthermore, the misorientation between the twin and parent grain in Fig. 6(c) is  $92^\circ$  about the  $\langle 23150 \rangle$  axis, and the lattice planes of the parent grain and twin are  $(4\bar{1}94)$  and  $(3\bar{1}43)$ , respectively. Thus, the deformation twin shown in Fig. 6(c) is confirmed as the  $\{172\}$  twin, almost no tolerance from the ideal misorientation relationship  $92^\circ$  about the  $\langle 1070 \rangle$  axis [19]. As reported, the  $\{130\}$  and  $\{172\}$  twins were extensively observed and confirmed in DU under plastic deformation due to low critical shear stress [20,21], thus, the  $\{130\}$  and  $\{172\}$  twins are also considered as the dominant twin modes in DU subjected to the dynamic deformation.

Besides twinning, other deformation mechanisms also play an important role in accommodating the severe plastic deformation due to fact that the shear displacement of the deformation twin is much smaller, leading to the fact that the shear strain accommodated by twinning is limited. The shear strain of the  $\{130\}$  and  $\{172\}$  twins are 0.299 and 0.227 [22], respectively, indicating that the accommodated shear strain by twinning is lower than 0.229. Thus, the severe plastic deformation

associated with shear strain larger than 0.299 needs other deformation mechanisms to trigger. In addition to deformation twins, dislocation, dislocation and twin interaction observed by TEM are shown in Figs. 7(b) and (c), indicating that dislocation slipping also plays an important role in DU under dynamic deformation. As reported, the  $[100](010)$  dislocation slipping was considered as a principal slip mode in DU [21], and other dislocation slip modes could be only triggered by high stress concentration zone and large strain localized zone. According to TEM observation of dislocation morphology, as shown in Fig. 7(b), the main dislocation slip mode can be distinguished as  $[100](010)$  dislocation slipping because of much larger crystal spacing. The principal dislocation slip mode  $[100](010)$  in DU represents only one independent slip system, thus multiple rational and irrational twin modes can be triggered to accommodate plastic deformation. The interaction of dislocation slipping and deformation twin can be observed in Fig. 7(c). When dislocation slipping cannot accommodate the plastic deformation of DU,

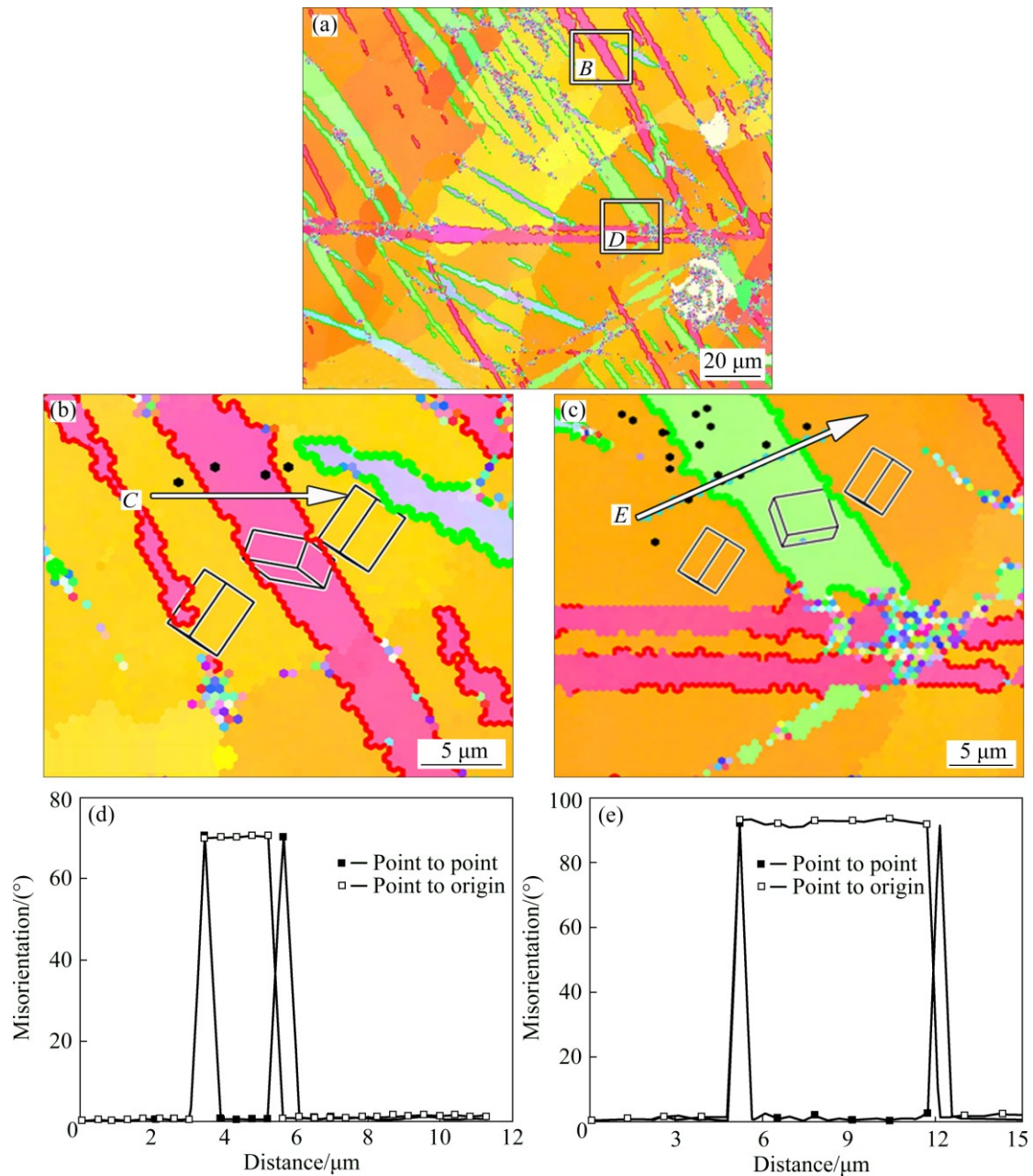


**Fig. 6** Twin mode analysis in depleted uranium target impacted at velocity of 50 m/s (red line: {130} twin; green line: {172} twin): (a) Inverse pole map; (b) High magnified map of {130} twin in zone B of Fig. 6(a); (c) High magnified map of {172} twin in zone D of Fig. 6(a); (d) Misorientation along line C in Fig. 6(b); (e) Misorientation along line E in Fig. 6(c)

which leads to stress concentration to trigger the formation of the deformation twins, the formation of the deformation twins can alter the crystal orientation, further resulting in the dislocation activated to accommodate the plastic deformation of DU. Thus, the interaction of dislocation slipping and deformation twin can improve plastic deformation ability of DU.

### 3.4 Microhardness of deformed microstructure

Microhardness distribution along impact direction from crater rim to deep matrix is measured, as shown in Fig. 8, and the measured distance from crater rim is

about 7 mm. It can be seen that the materials adjacent to the crater rim show the highest microhardness, about HV<sub>2</sub> 300. With increasing the distance from the crater rim, the microhardness values decrease gradually, as shown fit line in Fig. 8, indicating that plastic deformation level of DU is gradient variation from crater rim to deep matrix during high velocity impact. At deep matrix, the microhardness value is about HV<sub>2</sub> 200, 1/3 lower than that of the crater rim. The large fluctuation of the measured microhardness values can be observed, which should be associated with the inhomogeneous deformation and anisotropy of DU.

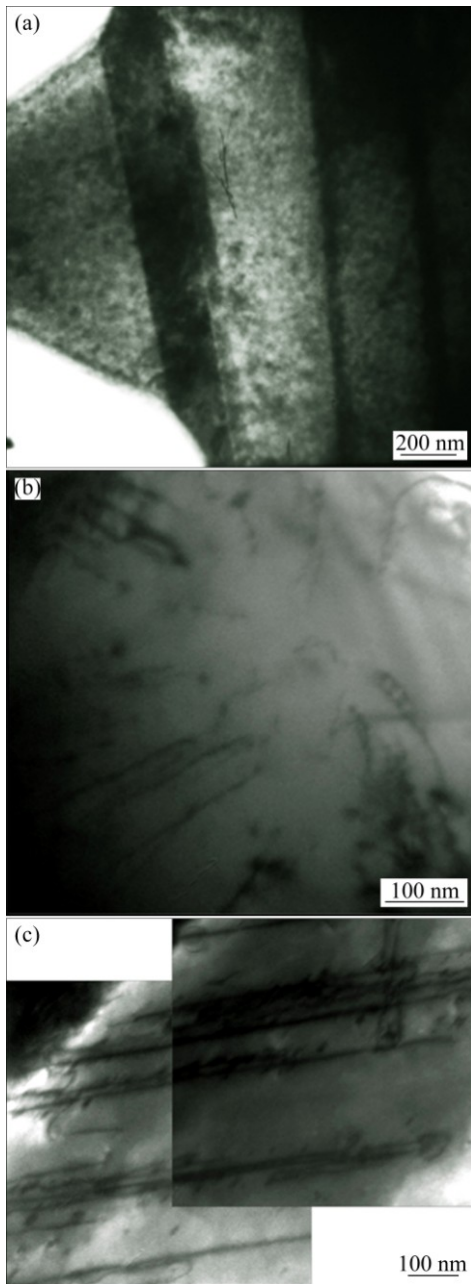


**Fig. 7** TEM images of deformed microstructure in depleted uranium target impacted by steel projectile at velocity of 50 m/s: (a) Deformation twin; (b) Dislocation; (c) Twin and dislocation interaction

**3.5 Deformed microstructure evolution**

Based on the characterization of deformed microstructure at different depths from the crater, the deformed microstructure evolution of DU under high velocity impact can be depicted, as shown in Fig. 9. At initial stage, {130}, {112} and {172} deformation twins are considered as the dominant plastic deformation mechanism of DU subjected to impact loadings, and the [100](010) dislocation slipping plays a assistant role, as shown in stage 1 of Fig. 9. With increasing the plastic strain, the secondary twins, even high-order twins, can be triggered by the localized stress concentration, as shown in stage 2 of Fig. 9. The formation of deformation twins alters the grain orientation, leading to a number of dislocations activated. Thus, dislocation slipping always plays an important role in DU under high velocity impact. At high strain rate and large strain stage, high density deformation twins can be intersected with each other, leading to the formation of the TFZ. At this time, high-order deformation twins are difficult to trigger because of small twin fragmentation laths and high critical shear stress, and high density dislocation can be activated in small twin fragmentation laths, slipping, interacting and piling up to form the sub-grains, as shown in stages 3 and 4 of Fig. 9. Finally, these

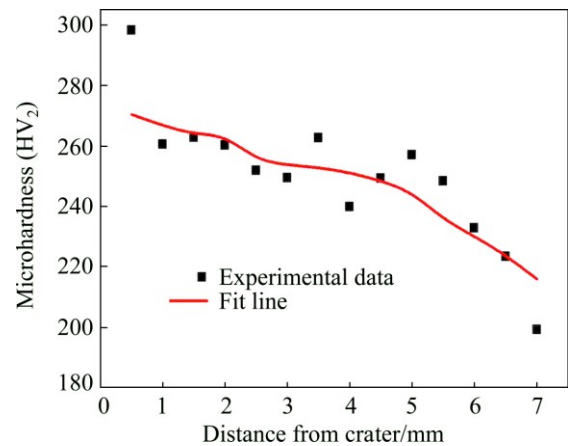


**Fig. 8** Microhardness distribution along impact direction in DU target impacted by steel projectile at velocity of 50 m/s

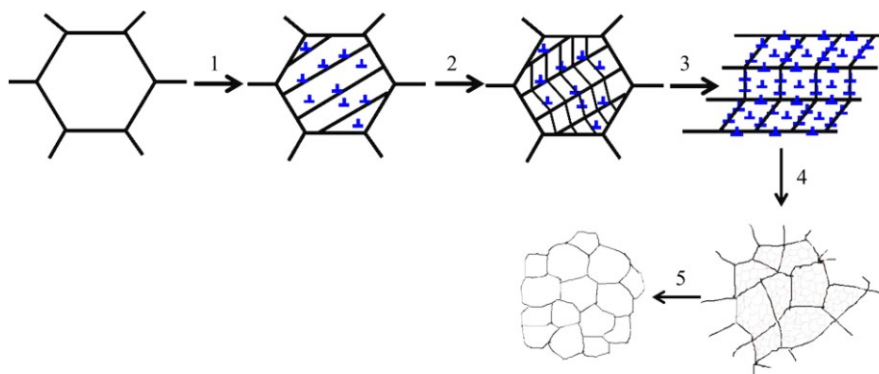


**Fig. 9** Deformed microstructure evolution model of depleted uranium under high velocity impact

sub-grains assisted with the temperature ring caused by plastic deformation lead to the occurrence of dynamic recrystallization to form randomly oriented dynamic recrystallized grains, as shown in stage 5 of Fig. 9.

## 4 Conclusions

1) Spherical cap crater can be formed in DU target impacted by steel projectile at a velocity of 50 m/s, and the diameter and depth of the impacted crater are 5.45 and 1.01 mm, respectively.

2) According to the twin density, four deformed zones can be divided from crater rim to deep matrix, and four deformed zones are twin fragmentation zone (zone I), high density deformation twin zone (zone II), low density deformation twin zone (zone III) and matrix zone (zone IV), respectively.

3) The {130} and {172} twins are considered as the dominant plastic deformation mechanism of DU subjected to impact loadings, and dislocation slipping also plays an important role in accommodating the dynamic plastic deformation of DU.

4) Based on the characterization of the microstructure at different depths from crater rim, deformed microstructure evolution of DU under high velocity impact is proposed.

## Acknowledgements

The authors wish to thank G. C. HU for providing the impact targets, Y. F. LI for TEM observation, and X. E. TANG for metallographic assistance.

## References

- [1] TOQUE C, MILODOWSKI A E, BAKER A C. The corrosion of depleted uranium in terrestrial and marine environments [J]. *Journal of Environmental Radioactivity*, 2014, 128: 97–105.
- [2] ZOU Dong-li, ZHEN Liang, ZHU Yao, XU Cheng-yan, SHAO Wen-zhu, PANG Bao-jun. Deformed microstructure evolution in AM60B Mg alloy under hypervelocity impact at a velocity of 5 km/s [J]. *Materials and Design*, 2010, 31: 3708–3715.
- [3] MURR L E, FERREYRA E T, PAPPU S, GARCIA E P, SANCHEZ J C, HUANG W, RIVAS J M, KENNEDY C, AYALA A, NIOU C S. Novel deformation process and microstructures involving ballistic penetrator formation and hypervelocity impact and penetration phenomena [J]. *Materials Characterization*, 1996, 37: 245–276.
- [4] MURR L E, AYALA A, NIOU C S. Microbands and shear-related microstructural phenomena associated with impact craters in 6061-T6 aluminum [J]. *Materials Science and Engineering A*, 1996, 216: 69–79.
- [5] MURR L E, NIOU C S, GARCIA E P, FERREYRA E T, RIVAS J M, SANCHEZ J C. Comparison of jetting-related microstructures associated with hypervelocity impact crater formation in copper targets and copper shaped charges [J]. *Materials Science and Engineering A*, 1997, 222: 118–132.
- [6] LEE W S, LIU C Y, SUN T N. Dynamic impact response and microstructural evolution of inconel 690 superalloy at elevated temperatures [J]. *International Journal of Impact and Engineering*, 2005, 32: 210–223.
- [7] MURR L E, TRILLO E A, BUJANDA A A, MARTINEZ N E. Comparison of residual microstructures associated with impact craters in fcc stainless steel and bcc iron targets: The microtwin versus microband issue [J]. *Acta Materialia*, 2002, 50: 121–131.
- [8] XUE Q, CERRETA E K, GRAY G T. Microstructural characteristics of post-shear localization in cold-rolled 316L stainless steel [J]. *Acta Materialia*, 2007, 55: 691–704.
- [9] KENNEDY C, MURR L E. Comparison of tungsten heavy-alloy rod penetration into ductile and hard metal targets: Microstructural analysis and computer simulations [J]. *Materials Science and Engineering A*, 2002, 325: 131–143.
- [10] ESQUIVEL E V, MURR L E. Grain boundary contribution to deformation and solidstate flow in severe plastic deformation [J]. *Materials Science and Engineering A*, 2005, 409: 13–23.
- [11] CHEN M W, MCCAULEY J W, HEMKER K J. Shock-induced localized amorphization in boron carbide [J]. *Science*, 2003, 299: 1563–1566.
- [12] CLARKE A J, FIELD R D, MCCABE R J, CADY C M, HACKENBERG R E, THOMA D J. EBSD and FIB/TEM examination of shape memory effect deformation structures in U-14at.%Nb [J]. *Acta Materialia*, 2008, 56: 2638–2648.
- [13] YANG Jin-wen, GAO Tao, LIU Ben-qiong, SUN Guang-ai, CHEN Bo. *Ab initio* calculation of the ideal tensile and shear strengths of uranium metal [J]. *Journal of Nuclear Materials*, 2015, 458: 122–128.
- [14] HILL M A, SCHULZE R K, BINGERT J F, FIELD R D, MCCABE R J, PAPIN P A. Filiform-mode hydride corrosion of uranium surfaces [J]. *Journal of Nuclear Materials*, 2013, 442: 106–115.
- [15] ZHANG Xu-hu, TANG Bin, ZHANG Xia-lu, KOU Hong-chao, LI Jin-shan, ZHOU Lian. Microstructure and texture of commercially pure titanium incold deep drawing [J]. *Transactions of Nonferrous Metals Society of China*, 2012, 22: 496–502.
- [16] LAN Yong-ting, ZHONG Xian-ci, QUAN Gao-feng, LIN Ruo-cheng, ZHANG Ke-shi. Crystal anisotropy of AZ31 magnesium alloy underuniaxial tension and compression [J]. *Transactions of Nonferrous Metals Society of China*, 2015, 25: 249–260.
- [17] GARLEA E, BRIDGES R L, GARLEA V O, CARPENTER D A, HEMPHILL M A, MORRELL J S. Characterization of a grain size refinement process in cast uranium [J]. *Materials Science and Engineering A*, 2013, 559: 210–216.
- [18] CHRISTIAN J W, MAHAJAN S. Deformation twinning [J]. *Progress in Materials Science*, 1995, 39: 1–157.
- [19] BINGERT J F, HANRANHAN R J, FIELD R D, DICKERSON P O. Microtextural investigation of hydrided  $\alpha$ -uranium [J]. *Journal of Alloys and Compounds*, 2004, 365: 138–148.
- [20] FIELD R D, MCCADE R J, ALEXANDER D J, TETER D F. Deformation twinning and twinning related fracture in coarse-grained  $\alpha$ -uranium [J]. *Journal of Nuclear Materials*, 2009, 392: 105–113.
- [21] MCCABE R J, CAPOLUNGO L, MARSHALL P E, CADY C M, TOME C N. Deformation of wrought uranium: Experiments and modeling [J]. *Acta Materialia*, 2010, 58: 5447–5459.
- [22] ZUEVA Y N, SAGARADZEB V V, PECHERKINAB N L, KABANOVAB I I, SVYATOVA I L, BONDARCHUKA S V, BELYAEVA D V. Phase and structural transformations in U and U-Nb alloy upon severe deformation and heat treatments [J]. *The Physics of Metals and Metallography*, 2013, 114: 1123–1154.

## 贫铀在钢弹 50 m/s 撞击下的显微组织演化

邹东利, 郭亚昆, 帅茂兵, 肖大武

中国工程物理研究院 材料研究所, 江油 621907

**摘要:** 通过激光共聚焦、背散射衍射、透射电子显微镜和显微压痕相结合的技术研究贫铀在钢弹 50 m/s 撞击下显微组织的演变过程。结果表明, 贫铀在钢弹撞击下会形成球冠状弹坑, 弹坑直径和深度分别为 5.45 和 1.01 mm。从弹坑边沿到基体内部, 变形组织可划分为 4 个区域: 孪晶碎化区、高密度孪晶区、低密度孪晶区和基体组织区。贫铀在动态变形过程中的主要塑性变形方式是孪生。除孪生外, 位错滑移在协调塑性变形时也发挥着重要作用。最后, 提出贫铀在高速撞击条件下显微组织的演变过程。

**关键词:** 贫铀; 钢弹; 动态变形; 显微组织演变; 孪生

(Edited by Wei-ping CHEN)